[10]CPP-Based Inclusion Complexes of Charged Fulleropyrrolidines. Effect of the Charge Location on the Photoinduced Electron Transfer

Olga A. Stasyuk,[a] Anton J. Stasyuk,*[a, b] Miquel Solà,*[a] and Alexander A. Voityuk*[a, c]

Abstract: A number of non-covalently bound donor-acceptor dyads, consisting of C_{60} as the electron acceptor and cyclo-paraphenylene (CPP) as the electron donor, have been reported. A hypsochromic shift of the charge transfer (CT) band in polar medium has been found in $\mathbf{[10]CPP{\supset}Li^+@C_{60}}$. To explore this anomalous effect, we study inclusion complexes $\mathbf{[10]CPP{\supset}Li^+@C_{60}\text{-MP}}$, $\mathbf{[10]CPP{\supset}C_{60}\text{-MPH}^+}$, and $\mathbf{[10]CPP{\supset}C_{60}\text{-PPyMe}^+}$ formed by fulleropyrrolidine derivatives and $\mathbf{[10]CPP}$ using the DFT/TDDFT approach. We show that the introduction of a positively charged fragment into fullerene stabilizes CT states that become the lowest-lying excited states. These charge-separated states can be generated by the decay of locally excited states on a nanosecond to picosecond time scale. The distance of the charged fragment to the center of the fullerenic cage and its accessibility to the solvent determine the strength of the hypsochromic shift.

Introduction

Cycloparaphenylenes (CPPs) and their analogs have received a lot of attention because of their unusual hoop-shaped structure with radially conjugated π-electron system.[1] As a result, significant advances in the synthesis of various CPPs have been observed over the past decade.[2] The diameter of the CPPs, which varies between 7 and 28 Å, is precisely controlled by the numbers of units in the macrocycle.[3] For this reason, CPPs are widely used in supramolecular chemistry.[4] The first host-guest complex of CPP was reported by Iwamoto et al. in 2011.[5] The authors found that [10]CPP with 10 phenylene units has a nearly ideal diameter (13.8 Å) to effectively accommodate the C_{60} fullerene. Keeping in mind that tuning the fullerene properties by functionalization is not a trivial task, a supramolecular approach to modifying the behavior of fullerenes appeared to be a very attractive method to obtain new fullerene-based systems. Over the next few years, dozens of new supramolecular complexes of CPP with various fullerenes and endohedral metallofullerenes have been reported.[6]

Among many complexes synthesized, the complexes based on ionic CPP are of particular interest. In 2013, Isobe and co-workers reported the synthesis and characterization of an inclusion complex of protonated N-methyl-fulleropyrrolidine in [4]cyclochrysenylene.[7] This system looks like carbon bearing in which fullerene rolls rapidly.[8] In 2015, Itami and co-workers successfully synthesized and characterized $\mathbf{[10]CPP{\supset}Li^+@C_{60}}$ complex.[9] Its structure was confirmed by X-ray crystallographic analysis. A Li^+ ion encapsulated in C_{60} drastically increases the ability of fullerene to accept electrons and facilitate the charge transfer from CPP to the fullerene cage.

We have recently shown that the encapsulation of Li^+ with fullerene in $[10]CPP{\supset}C_{60}$ resulting in $\mathbf{[10]CPP{\supset}Li^+@C_{60}}$ leads to considerable changes in electronic structure.[10] In particular, the HOMO-LUMO gap decreases by 1 eV. A similar decrease in energy from 2.50 to 1.72 eV was found for the lowest singlet excited state. These and other changes are associated with the electrostatic stabilization of the charge transfer state by Li^+. Moreover, an unusual destabilization of charge transfer (CT) states generated by photoexcitation in a polar medium was found for this complex. In turn, this is accompanied by a blue (i.e., hypsochromic) shift of the CT band and an anomalous dependence of the electron transfer rate on the polarity of the medium.

In this article, we describe a comprehensive analysis based on time-dependent density functional theory (TD-DFT) calculations of several inclusion complexes of [10]CPP with fulleropyrrolidine derivatives in order to explore the effect of the location of a positive charge in the supramolecules on their photoinduced electron transfer (PET) properties.

[a] Dr. O. A. Stasyuk, Dr. A. J. Stasyuk, Prof. M. Solà, Prof. A. A. Voityuk
     Institut de Química Computacional and Departament de Química
     Universitat de Girona
     C/ Maria Aurèlia Capmany 69, 17003 Girona (Spain)
     E-mail: antony.stasuk@gmail.com
            miquel.sola@udg.edu
            alexander.voityuk@icrea.cat

[b] Dr. A. J. Stasyuk
     Faculty of Chemistry, University of Warsaw, Pasteura 1, 02-093 Warsaw
     (Poland)

[c] Prof. A. A. Voityuk
     Institució Catalana de Recerca i Estudis Avancats (ICREA), 08010 Barcelona
     (Spain)

⌨ Supporting information for this article is available on the WWW under
   https://doi.org/10.1002/chem.202005516

Chemistry–A European Journal

Full Paper
doi.org/10.1002/chem.202005516

Chemistry
Europe
European Chemical
Societies Publishing

Results and Discussion

Structure and relative stability of [10]CPP-fulleropyrrolidine inclusion complexes

We consider one neutral and three positively charged complexes of fulleropyrrolidines in [10]CPP. The neutral *N*-methylfulleropyrrolidine complex ([10]CPP⊃C_{60}-MP) is our reference. Other three complexes differ from each other by the location of the positive charge. In [10]CPP⊃Li$^+$@C_{60}-MP, the charge is located inside the fullerene cage, almost in the center of the complex. In [10]CPP⊃C_{60}-MPH$^+$, the protonated form of N-methylfulleropyrrolidine is used, and thus the charge is located near the fullerene. Finally, in [10]CPP⊃C_{60}-PPyMe$^+$, where the methyl group is replaced with N-methylpyridinium, the positive charge is shifted from the fullerene to the CPP unit (Figure 1).

As seen in Figure 1, the HOMO and LUMO energies of neutral and charged complexes differ significantly. In the neutral [10]CPP⊃C_{60}-MP complex, HOMO is localized on [10]CPP and its energy is similar to that of the isolated cycloparaphenylene host (−6.53 and −6.57 eV, respectively). The LUMO is localized on C_{60}-MP and its energy is higher by 0.24 eV than in the free fulleropyrrolidine. In contrast, the formation of charged complexes is accompanied by sharp changes in the HOMO energy. The maximum shift of the HOMO energy (1.88 eV) is found in [10]CPP⊃Li$^+$@C_{60}-MP, while the minimum shift (1.51 eV) is found in [10]CPP⊃C_{60}-PPyMe$^+$ (see Table S1, Supporting Information). These changes are caused by the electrostatic effect of the positive charge. In Li$^+$@C_{60}-MP, almost all the charge is localized on Li$^+$. In C_{60}-MPH$^+$ and C_{60}-PPyMe$^+$, the charge is mainly localized on the protonated N-methyl-pyrrolidine group and pyridinium cation, respectively. Thus, in this series, the effective distance between [10]CPP and the positive charge gradually increases, which leads to a decrease of the electrostatic effect. The LUMO energies also change (from 0.54 to 0.22 eV) though to a smaller extent than the HOMO energies. Interestingly, an almost equal LUMO energy shift is found in neutral [10]CPP⊃C_{60}-MP and charged [10]CPP⊃C_{60}-PPyMe$^+$ complexes (0.24 and 0.22 eV, respectively), which indicates the absence of charge separation in the ground state. Indeed, the population analysis of the systems (Table S2, Supporting Information) does not reveal any significant charge transfer between the host and guest molecules.

To estimate the stability of the complexes, the interaction energy (ΔE_{int}) between [10]CPP and fulleropyrrolidine units was computed. For [10]CPP⊃C_{60}-MP, [10]CPP⊃Li$^+$@C_{60}-MP, [10]CPP⊃C_{60}-MPH$^+$, and [10]CPP⊃C_{60}-PPyMe$^+$ systems, ΔE_{int} is found to be −56.1, −66.4, −62.4, and −62.8 kcal/mol, correspondingly. ΔE_{int} in the neutral complex is less than in the charged ones, where the interaction energies are quite close. To analyze the nature of the host-guest interactions, we performed the energy decomposition analysis (EDA) proposed by Morokuma[11] as implemented in ADF.[12] The EDA decomposes the interaction energy into four components: electrostatic (ΔE_{elstat}), Pauli repulsion (ΔE_{Pauli}), orbital (ΔE_{oi}), and dispersion correction (ΔE_{disp}), and allows one to estimate the role of specific interactions. The EDA data listed in Table 1 indicate that the host-guest interactions in the systems are similar.

The destabilizing term – the Pauli repulsion varies from 77 to 87 kcal mol^{-1}. Among the binding forces ($\Delta E_{elstat} + \Delta E_{oi} + \Delta E_{disp}$), the dispersion term prevails, with a contribution of more than 60%. The second largest term is electrostatic with a
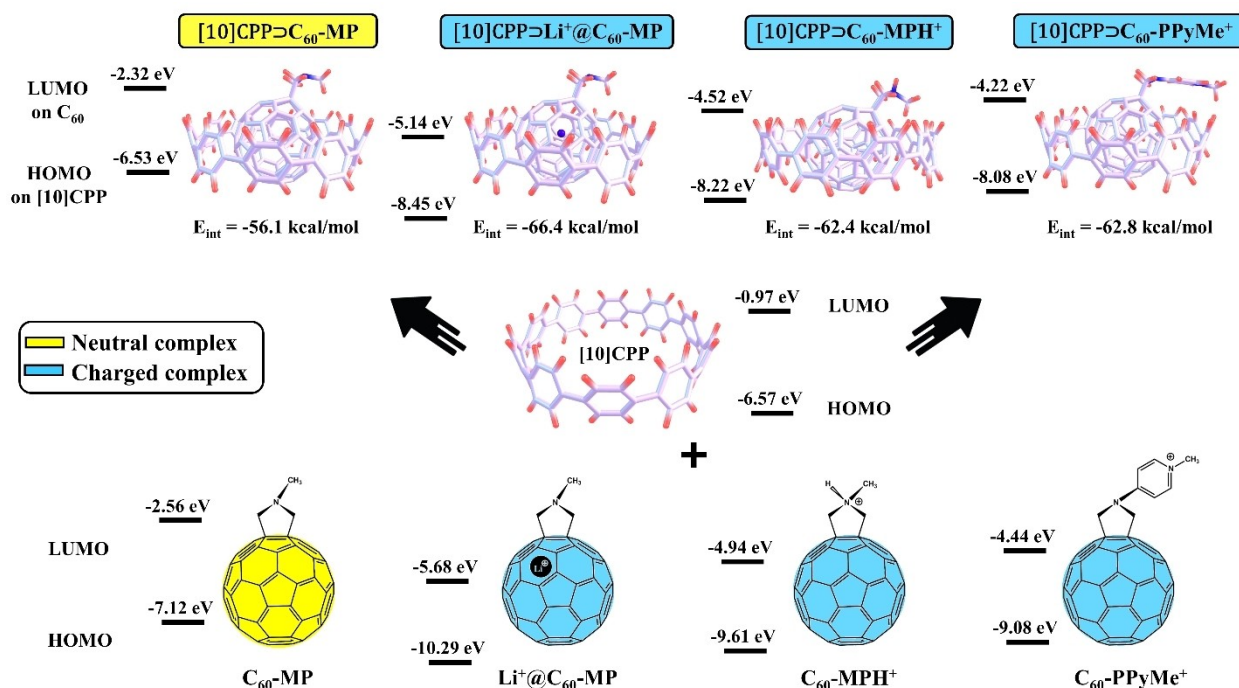

Figure 1. Structures, HOMO and LUMO energies, and interaction energies (E$_{int}$) of the studied complexes.

Table 1. EDA results for [10]CPP⊃C_{60}-MP, [10]CPP⊃Li^+@C_{60}-MP, [10]CPP⊃C_{60}-MPH^+, and [10]CPP⊃C_{60}-$PPyMe^+$ complexes.[a]

Complex	Energy terms				
	ΔE_{Pauli}	ΔE_{elstat}	ΔE_{oi}	ΔE_{disp}	ΔE_{int}
[10]CPP⊃C_{60}-MP	80.03	−34.42 (25.3%)	−14.65 (10.8%)	−87.10 (64.0%)	−56.14
[10]CPP⊃Li^+@C_{60}-MP	77.71	−34.87 (24.2%)	−21.46 (14.9%)	−87.80 (60.9%)	−66.42
[10]CPP⊃C_{60}-MPH^+	82.19	−33.05 (22.9%)	−20.60 (14.3%)	−90.91 (62.9%)	−62.37
[10]CPP⊃C_{60}-$PPyMe^+$	86.95	−34.51 (23.0%)	−20.66 (13.8%)	−94.57 (63.2%)	−62.79

[a] The energy values are in kcal mol^{-1}. The percentage contributions to the sum of all attractive energy terms are given in parentheses.

contribution of 23–25%. Orbital interactions provide no more than 15%. Their contribution slightly changes in the line [10]CPP⊃Li^+@C_{60}-MP, [10]CPP⊃C_{60}-MPH^+, and [10]CPP⊃C_{60}-$PPyMe^+$, which indicates an increase in the HOMO-LUMO gap (Table S1) and reducing the charge transfer in the ground state (Table S2).

Singlet excited states

The simulations of the lowest 100 excited states were carried out by the TDA-DFT method with the CAM-B3LYP-D3(BJ)/def2-SVP//BLYP-D3(BJ)/def2-SVP scheme. The electronic density of the excited states was analyzed in terms of the guest C_{60}-XXX and the host [10]CPP contributions. Three types of the excited states were identified:
(1) Locally excited (LE) states, in which the excitation is mainly localized on one fragment, with a charge separation value

CS < 0.1e. Within the studied excited states, only LE excitations on the fullerene moiety (LE^{Guest}) are found.
(2) Charge transfer (CT) states with the electron density transferred between the fragments (CS > 0.9e)
(3) Mixed states with a significant contribution of both LE and CT (0.1e < CS < 0.9e).

In the gas phase, 100 lowest vertical singlet excitation energies of [10]CPP⊃C_{60}-MP vary from 2.41 to 4.80 eV. The analysis revealed that the first excited state at 2.41 eV is the LE state on C_{60}-MP unit (LE^{Guest}) and corresponds to the HOMO-1→LUMO excitation. The lowest CT state (with 0.98 e transferred between the subunits) lies higher in energy, at 2.93 eV, and corresponds to the HOMO→LUMO+1 transition. The CT state can be described as [10]CPP^+⊃C_{60}-MP^-. Among the studied excited states, only this type of charge separated states was observed (Table 2).

For the charged complexes [10]CPP⊃Li^+@C_{60}-MP, [10]CPP⊃C_{60}-MPH^+, and [10]CPP⊃C_{60}-$PPyMe^+$, the energy of the LE^{Guest} state (HOMO-3→LUMO) is almost the same as that of the neutral. In contrast to [10]CPP⊃C_{60}-MP, the lowest excited state in the charged complexes corresponds to the CT state formed due to electron transfer from [10]CPP to the fullerene moiety. Also, a notable decrease in the HOMO-LUMO (HL) energy gap is found (Table S1). When passing from the neutral complex [10]CPP⊃C_{60}-MP to its Li^+-doped analog, the HL gap drops from 4.21 to 3.31 eV. We note that the changes in the band gap become smaller as the positive charge moves away from the center of the complex. In [10]CPP⊃C_{60}-$PPyMe^+$, in which the charge is far from the center, the HL gap is 3.86 eV. The fact that the introduction of the positive charge does not affect the energy of LE states but strongly affects the CT states, clearly indicates the electrostatic nature of the observed effect. Such stabilization of CT state was previously reported for the experimentally and theoretically studied [10]CPP⊃Li^+@C_{60}

Table 2. Excitation energies (E_x, eV), main singly excited configuration (HOMO(H)−LUMO(L)) and its weight (W), oscillator strength (f), extent of charge transfer (CT, e) or localization of exciton (X) in the host-guest systems.

	Supramolecular host-guest systems			
	[10]CPP⊃C_{60}-MP	[10]CPP⊃Li^+@C_{60}-MP	[10]CPP⊃C_{60}-MPH^+	[10]CPP⊃C_{60}-$PPyMe^+$
	LE^{Guest} (Fullerene C_{60}-XXX)			
E_x	2.412	2.452	2.445	2.467
Transition (W)	H-1-L (0.80)	H-3-L (0.81)	H-3-L (0.85)	H-3-L (0.79)
f	0.004	0.003	0.001	0.002
X	0.951	0.895	0.937	0.903
	Most absorptive transition			
E_x	3.858	3.835[a]	3.841[a]	3.867[a]
Transition (W)	H-3-L+3 (0.17)	H-1-L+4 (0.18)	H-L+8 (0.22)	H-L+10 (0.10)
f	0.712	0.236	0.734	0.493
Localization	[10]CPP/C_{60}-XXX	[10]CPP/C_{60}-XXX	[10]CPP/C_{60}-XXX	[10]CPP/C_{60}-XXX
X	0.68/0.24	0.22/0.12	0.61/0.10	0.40/0.28
CT	0.08	0.66	0.29	0.32
	CT ([10]CPP→C_{60}-XXX)			
E_x	2.934	1.864	2.275	2.416
Transition (W)	H-L+1 (0.93)	H-L (0.94)	H-L (0.91)	H-L (0.88)
f	0.001	0.005	0.011	0.007
CT	0.98	0.99	0.98	0.92

[a] - mixed state with significant contributions of both LE and CT.

Chemistry–A European Journal

Full Paper
doi.org/10.1002/chem.202005516

Chemistry Europe
European Chemical
Societies Publishing

complex,[10] as well as for Li$^+$-doped carbon nano-onions[13] and the Zn-porphyrin–[10]CPP⊃C$_{60}$ junction.[14] An important point is that excited states with a high oscillator strength are found in each system. In [10]CPP⊃C$_{60}$-MP, these are LE states delocalized both in the host and in the guest fragments. The highly absorptive states in the charged complexes are mixed states. The Kohn-Sham molecular orbitals for the LE^{Guest} and CT states are shown in Figures S1-S4, Supporting Information.

Solvent effects

A well-proven COSMO-like model in monopole approximation with dichloromethane (DCM) as the solvent was applied to estimate the effect of polar environment on electronic excitations.[15] The ground state (GS) solvation energies of **[10]CPP⊃C$_{60}$-MP**, **[10]CPP⊃Li$^+$@C$_{60}$-MP**, **[10]CPP⊃C$_{60}$-MPH$^+$**, and **[10]CPP⊃C$_{60}$-PPyMe$^+$** complexes are −0.11, −1.13, −2.11, and −1.75 eV, respectively. As expected, the solvation energy of the charged complexes are noticeably larger in comparison with **[10]CPP⊃C$_{60}$-MP**. The difference in solvation energies for **[10]CPP⊃Li$^+$@C$_{60}$-MP** and other charged systems can be explained by shielding of the positive charge of Li$^+$ by the fullerene cage and its isolation from the solvent.[16] On the contrary, in **[10]CPP⊃C$_{60}$-MPH$^+$** and **[10]CPP⊃C$_{60}$-PPyMe$^+$**, the charge is localized on the pyrrolidinium moiety and, thus, accessible to the solvent. The solvation energy of **[10]CPP⊃C$_{60}$-PPyMe$^+$** is 0.36 eV lower than that of **[10]CPP⊃C$_{60}$-MPH$^+$** due to the higher delocalization of the positive charge. The difference in the dipole moments of the GS and LE^{Guest} states is rather small and does not exceed 2D. As expected, the solvation energies of LE^{Guest} states are very similar to that of the GS. Detailed data for all complexes are given in Table S3, Supporting Information.

Usually, the dipole moments of CT states are significantly larger than those of LE states. However, high ability of the both fragments to effective charge delocalization gives a reason for a relatively small difference in the dipole moments of the GS and CT states. Calculations showed that in **[10]CPP⊃C$_{60}$-MP** this difference is only 2.6D and the energy of CT state changes from 2.93 to 2.61 eV leading to a bathochromic shift of CT band by about 50 nm. The stabilization of the CT state by solvent is insufficient, however, to reorder the CT and LE states. In the charged complexes, a hypsochromic shift is observed. Our modeling reveals that the magnitude of the "blue" shift is inversely proportional to the distance from the positive charge to the center of the complex. In **[10]CPP⊃Li$^+$@C$_{60}$-MP**, where the charge is localized almost in the center of the complex, the hypsochromic shift is maximal and equal to 0.23 eV. In **[10]CPP⊃C$_{60}$-PPyMe$^+$**, the shift is small (0.04 eV). Figure 2 displays the energies of GS, LE, and CT states in the studied complexes.

Thus, the introduction of a charged fragment into the **[10]CPP** inclusion complexes stabilizes the CT state and makes it the lowest excited state. This leads to the energetically favorable charge separation.

To get a more quantitative insight into the solvent effects, we performed the excited state simulations for various solvents with dielectric constant ranging from $\varepsilon \approx 2$ (toluene) to $\varepsilon \approx 25$
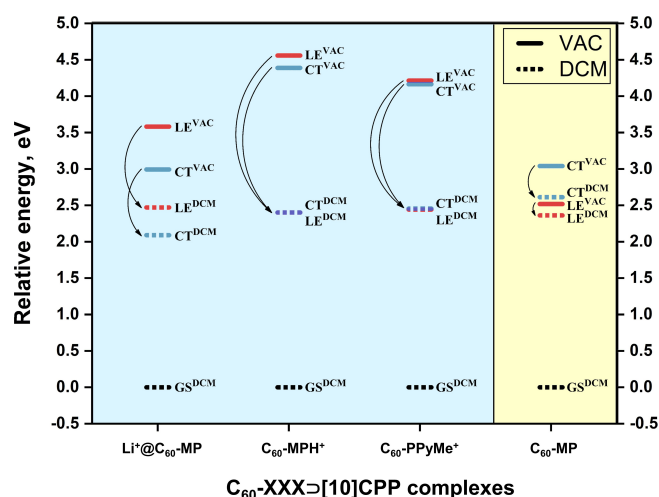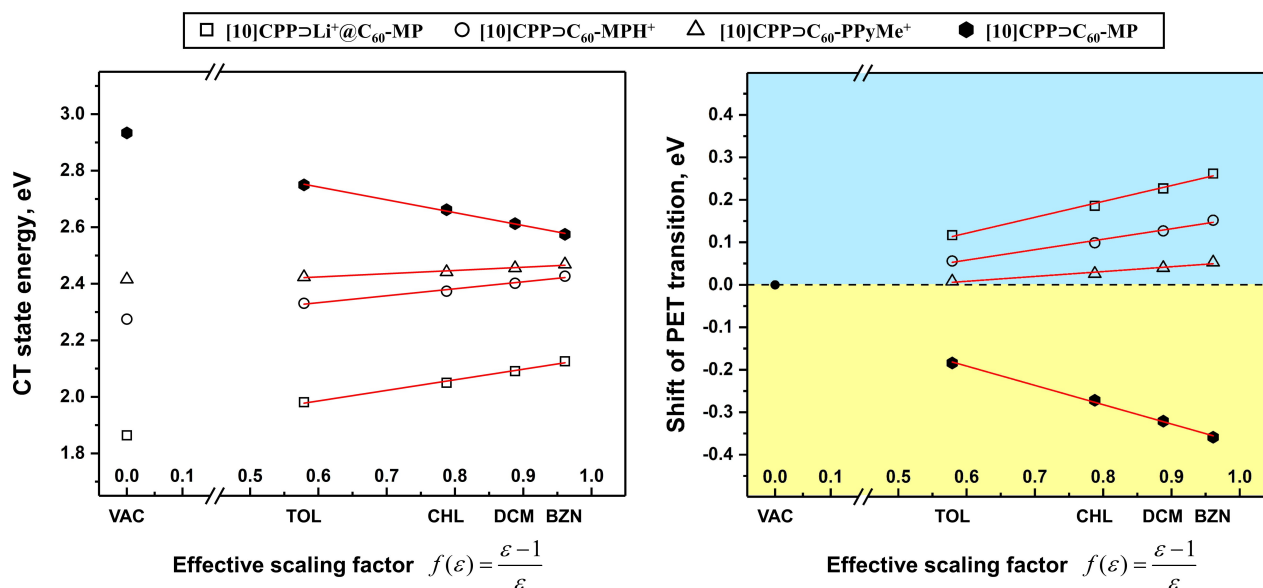

Figure 2. Relative energies (in eV) of GS, LE, and CT states of [10]CPP⊃C$_{60}$-MP, [10]CPP⊃Li$^+$@C$_{60}$-MP, [10]CPP⊃C$_{60}$-MPH$^+$, and [10]CPP⊃C$_{60}$-PPyMe$^+$ complexes computed in vacuum (VAC) and dichloromethane (DCM). The charged systems are highlighted in blue, and the neutral complex in yellow.

(benzonitrile). In all cases, the gas-phase geometry was used to avoid any effect associated with the geometry alteration. In all solvents, LE^{Guest} and GS states demonstrate similar solvation energies. However, the behavior of CT state strongly depends on the solvent polarity. As seen in Figure 3, [10]CPP⊃Li$^+$@C$_{60}$-MP complex exhibits a pronounced (about 0.26 eV) hypsochromic shift when going from the gas-phase to the polar solvent. Detailed data for the solvation energies of complexes are given in Table S4, Supporting Information).

Solvation of neutral molecules and ions within the polarized continuum model is determined by electrostatic (E$_{el}$) and non-electrostatic (E$_{non-el}$) contributions. The last component, in turn, consists of three main terms including dispersion (E$_{vdW}$), repulsion (E$_{rep}$) and cavitation (E$_{cav}$) energies.[17] Because the geometry does not change during a vertical excitation, the difference in the solvation energy will be determined only by E$_{el}$. To explain the observed hypsochromic shift, the molecular electrostatic potential (MEP) of the charged complexes in their GS and CT states was calculated (Figure 4).

Figure 4 demonstrates a qualitative difference between the MEP of **[10]CPP⊃Li$^+$@C$_{60}$-MP** and the MEPs of **[10]CPP⊃C$_{60}$-MPH$^+$** and **[10]CPP⊃C$_{60}$-PPyMe$^+$**. For the Li$^+$-doped system, the positive charge is located inside the fullerene, while for the other two molecules the positive charge is localized on pyrrolidine/pyridinium fragment. Upon the electron transfer (ET) from **[10]CPP** to Li$^+$@C$_{60}$, the fullerene subunit becomes almost neutral, decreasing the MEP around this fragment. In **[10]CPP⊃C$_{60}$-PPyMe$^+$**, the most noticeable changes caused by ET occur on the pyrrolidino-pyridinium fragment, whereas the fullerene cage remains almost unchanged. In **[10]CPP⊃C$_{60}$-MPH$^+$** there are some changes both on pyrrolidine and on fullerene. The MEP changes around **[10]CPP** are rather small due to the efficient delocalization of the positive charge. Thus, the hypsochromic shift of the CT band is caused by MEP changes on the guest moiety. Changes of the MEP in neutral

Chemistry–A European Journal

Full Paper
doi.org/10.1002/chem.202005516

Chemistry Europe
European Chemical
Societies Publishing

Figure 3. Left: CT excited state energies for **[10]CPP⊃C$_{60}$-MP**, **[10]CPP⊃Li$^+$@C$_{60}$-MP**, **[10]CPP⊃C$_{60}$-MPH$^+$**, and **[10]CPP⊃C$_{60}$-PPyMe$^+$** systems as a function of solvent polarity. Right: Solvent dependent shifts of PET transition energy for the studied complexes in selected solvents (TOL = toluene; CHL = chloroform; DCM = dichloromethane, and BZN = benzonitrile).
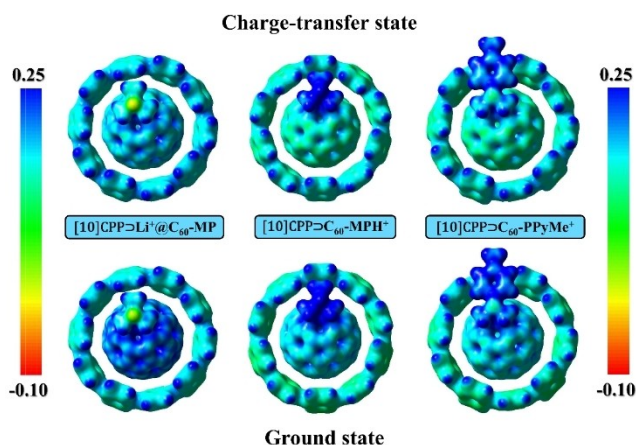
Figure 4. Calculated molecular electrostatic potential surface for **[10]CPP⊃Li$^+$@C$_{60}$-MP**, **[10]CPP⊃C$_{60}$-MPH$^+$**, and **[10]CPP⊃C$_{60}$-PPyMe$^+$** in the ground state (bottom) and the CT state (top). The surfaces are drawn at electron density contours of 0.03 e Å^{-3}, and colored according to the electrostatic potential value.

[10]CPP⊃C$_{60}$-MP complex occur mostly on fullerene unit, while in the methyl pyrrolidine fragment are minimal (Figure S5, Supporting Information).

Electron transfer rates

GS→CT transitions have typically a very weak oscillator strength and thus the CT states cannot be well populated by light absorption. However, they can be generated by a decay of LE states. The rates of electron transfer (k_{ET}) and charge recombination (k_{CR}) were calculated using the semi-classical method by

Ulstrup and Jortner.[18] Within this approach, the intramolecular relaxation associated with ET is described by an effective vibrational mode, and the rate is controlled by four parameters: electronic coupling (V_{ij}) of the initial and the final states, solvation reorganization energy λ_s, reaction Gibbs energy ΔG^0, and effective Huang-Rhys factor S_{eff}. The computed parameters, as well as k_{ET} and k_{CR} rates in DCM are listed in Table 3. The rates were computed using the effective frequency of 1600 cm^{-1}, which corresponds to the stretching of C=C bonds. Note that the calculated charge separation rates for nanoring-fullerene inclusion complexes do not change significantly by varying the effective frequency from 1400 to 1800 cm^{-1}.[19]

Charge separation in neutral **[10]CPP⊃C$_{60}$-MP** is characterized by a positive ΔG^0 value. The estimated CT rate for this complex is rather low (9.17·10^5 s^{-1}), and thus photoinduced electron transfer is unlikely to be observed in this system. For **[10]CPP⊃C$_{60}$-MPH$^+$** and **[10]CPP⊃C$_{60}$-PPyMe$^+$**, PET occurs in normal Marcus regime ($|\Delta G^0| < \lambda$), while for Li$^+$-doped **[10]CPP⊃Li$^+$@C$_{60}$-MP**, the PET reaction takes place in the inverted Marcus region ($|\Delta G^0| > \lambda$). Charge separation in **[10]CPP⊃C$_{60}$-MPH$^+$** and **[10]CPP⊃C$_{60}$-PPyMe$^+$** occurs in picosecond timescale (the characteristic time is 21 and 7 ps, respectively). The ET rate in **[10]CPP⊃Li$^+$@C$_{60}$-MP** is lower, the reaction takes place in nanosecond time scale (Table 3). The charge recombination reaction occurs in the inverted Marcus regime ($|\Delta G_0| \gg \lambda$) and is significantly slower than the charge separation.

Conclusions

Photoinduced electron transfer has been studied in a series of inclusion complexes of fulleropyrrolidines in **[10]CPP** using the TD-DFT approach. In this work, we have demonstrated that the

Chemistry–A European Journal

Full Paper
doi.org/10.1002/chem.202005516

Chemistry Europe
European Chemical
Societies Publishing

Table 3. Gibbs energy ΔG^0 (in eV), electronic coupling V_{ij} (in eV), solvent (λ_s) and internal (λ_i) reorganization energy (in eV), Huang–Rhys factor (S_{eff}) and rates k_X (in s^{-1}) for ET and CR processes in **[10]CPP⊃C$_{60}$-MP**, **[10]CPP⊃Li$^+$@C$_{60}$-MP**, **[10]CPP⊃C$_{60}$-MPH$^+$**, and **[10]CPP⊃C$_{60}$-PPyMe$^+$** complexes computed in DCM.

[10]CPP⊃C$_{60}$-XXX	Transition	$\Delta G^{0[a]}$ [eV]	$\lvert V_{ij}\rvert$ [eV]	Reorg. Energy [eV]		$S_{eff}^{[b]}$	k_X [s^{-1}]
				λ_i	λ_s		
Li$^+$@C$_{60}$-MP	LE→CT	−0.381	2.48·10^{-4}	0.136	0.172	0.685	1.11·10^9
	CT→GS	−2.091	1.17·10^{-4}	0.162	0.171	0.818	4.91·10^1
C$_{60}$-MPH$^+$	LE→CT	0.000	3.09·10^{-3}	0.141	0.204	0.709	4.89·10^{10}
	CT→GS	−2.402	7.41·10^{-4}	0.162	0.172	0.804	5.54·10^1
C$_{60}$-PPyMe$^+$	LE→CT	0.013	5.23·10^{-3}	0.164	0.177	0.828	1.50·10^{11}
	CT→GS	−2.456	2.19·10^{-2}	0.160	0.204	0.988	1.15·10^5
C$_{60}$-MP	LE→CT	0.250	7.36·10^{-4}	0.156	0.171	0.789	9.17·10^5
	CT→GS	−2.613	1.17·10^{-3}	0.196	0.177	0.815	5.16·10^0

[a] Gibbs energy difference between the denoted states in DCM. [b] An effective value of the Huang–Rhys factor $S_{eff}=\lambda_i/\hbar\omega_{eff}$, where $\hbar\omega_{eff}$ is set to 1600 cm^{-1}.

introduction of a positive charge into fullerene unit leads to the stabilization of CT states, which become the lowest. The charge inside the fullerene cage results in a substantial hypsochromic shift of the CT band. However, the effect decreases rapidly as the charge becomes more accessible to the solvent. The formation of charge separated states by electron transfer from **[10]CPP** to **C$_{60}$-MP** in the neutral complex is found to be slow, making the PET unlikely. In contrast, charge separated states in the charged complexes **[10]CPP⊃Li$^+$@C$_{60}$-MP**, **[10]CPP⊃C$_{60}$-MPH$^+$**, and **[10]CPP⊃C$_{60}$-PPyMe$^+$** can be generated by the decay of the lowest LE states.

Computational details

Quantum-chemical calculations

Geometry optimization of the complexes was performed employing the DFT BLYP[20] exchange − correlation functional with Ahlrichs' def2-SVP basis set,[21] and using the resolution of identity approximation (RI, alternatively termed as density fitting)[22] implemented in the ORCA 4.2.1 program.[23] The host-guest interaction energy was computed using BLYP functional coupled with triple-ξ def2-TZVP basis set.[21b] Vertical excitation energies were calculated using TDA formalism[24] with the range-separated CAM-B3LYP functional from Handy and coworkers,[25] and Ahlrichs' def2-SVP basis set, using Gaussian 16 (rev. A03).[26] The empirical dispersion D3 correction with Becke-Johnson damping[27] was employed. To visualize molecular structures and orbitals, Chemcraft 1.8 program[28] was used.

Analysis of excited states

The quantitative analysis of exciton delocalization and charge transfer in the donor-acceptor complexes is carried out in terms of the transition density.[29] The analysis is convenient to perform in the Löwdin orthogonalized basis. The matrix $^\lambda$**C** of orthogonalized MO coefficients is obtained from the coefficients **C** in the original basis $^\lambda$**C** = **S**$^{1/2}$ **C**, where **S** is the atomic orbital overlap matrix. The transition density matrix T^{0i} for an excited state Φ_i is constructed as a superposition of singly excited configurations (where an occupied MO ψ_j is replaced by a virtual MO ψ_a) [Eq. (1)]:

$$T^{0i}_{\alpha\beta} = \sum_{ja} A^i_{j\to a} \,{}^\lambda C^\lambda_{\alpha j} C_{\beta a} \tag{1}$$

where $A^i_{j\to a}$ is the expansion coefficient of the j→a configuration in the Φ_i and α and β are atomic orbitals.

A key quantity $\Omega(D,A)$ is determined by [Eq. (2)]:

$$\Omega(D,A) = \sum_{\alpha\in D,\,\beta\in A} \left(T^{0i}_{\alpha\beta}\right)^2 \tag{2}$$

The weights of local excitations on D and A are $\Omega(D,D)$ and $\Omega(A,A)$. The weight of electron transfer configurations D→A and A→D is represented by $\Omega(D,A)$ and $\Omega(A,D)$, respectively. The index Δq, which describes charge separation and charge transfer between D and A, is [Eq. (3 and 4)]:

$$\Delta q(CS) = \sum \Omega(D,A) - \Omega(A,D) \tag{3}$$

$$\Delta q(CT) = \sum \Omega(D,A) + \Omega(A,D) \tag{4}$$

Solvent effects

The equilibrium solvation energy of a molecule (in the ground or excited state) in a solvent with dielectric constant ε was estimated using a COSMO-like polarizable continuum model[15a,30] in monopole approximation [Eq. (5)]:

$$E^{eq}_S(Q,\varepsilon) = -\frac{1}{2}f(\varepsilon)Q^+DQ \tag{5}$$

where $f(\varepsilon)$ is the dielectric scaling factor, $f(\varepsilon)=1-1/\varepsilon$, **Q** is the vector of n atomic charges in the molecular system, **D** is the n x n symmetric matrix determined by the shape of the boundary surface between solute and solvent. **D** = **B**$^+$**A**$^{-1}$**B**, where the m x m matrix **A** describes electrostatic interaction between m surface charges and the m x n **B** matrix describes the interaction of the surface charges with n atomic charges of the solute.[15a,30] The GEPOL93 scheme[31] was used to construct the molecular boundary surface.

The charge on atom X in the excited state Φ_i is calculated as [Eq. (6)]:

$$q^i_X = q^0_X + \Delta^i_X, \quad \Delta^i_X = \frac{1}{2}\sum_{Y\neq X}\sum_{\alpha\in X,\,\beta\in Y}(T^{0i}_{\alpha\beta}T^{0i}_{\alpha\beta} - T^{0i}_{\beta\alpha}T^{0i}_{\beta\alpha}), \tag{6}$$

where q^0_X is the atomic charge on atom X in the ground state and Δ^i_X is its change due to redistribution of the electron density caused by the excitation $\psi_0\to\psi_i$.

Chemistry–A European Journal

Full Paper
doi.org/10.1002/chem.202005516

Chemistry Europe
European Chemical
Societies Publishing

The non-equilibrium solvation energy for excited state ψ_i can be estimated as [Eq. (7)]:[32]

$$E_S^{neq}(Q^0, \Delta, \varepsilon, n^2) = f(\varepsilon)\Delta^+ D Q^0 - \frac{1}{2}f(n^2)\Delta^+ D\Delta. \qquad (7)$$

In Equation (7), n^2 (the refraction index squared) is the optical dielectric constant of the medium and the vector Δ describes the change of atomic charges in the molecule by excitation in terms of atomic charges, see Equation (6).

Electron transfer rates

The rate of nonadiabatic ET, k_{ET}, can be expressed in terms of the electronic coupling squared, V^2, and the Franck–Condon Weighted Density of states (FCWD) [Eq. (8)]:

$$k_{ET} = \frac{2\pi}{\hbar}V^2 \, (FCWD) \qquad (8)$$

that accounts for an overlap of vibrational states of donor and acceptor, and can be approximately estimated using the classical Marcus equation [Eq. (9)]:[33]

$$(FCWD) = (4\pi\lambda kT)^{-1/2} \exp\left[-(\Delta G^0 + \lambda)^2 / 4\lambda kT\right] \qquad (9)$$

where λ is the reorganization energy and ΔG^0 is the standard Gibbs energy change of the process. The fragment charge difference (FCD)[34] method was employed to calculate the electronic couplings in this work.

The Marcus expression is derived for the high-temperature condition, $\hbar\omega_l \ll kT$, for all vibrational modes l. The semi-classical description of ET[18,35] includes the effect of quantum vibrational modes in an effective way, the solvent (low frequency) modes are treated classically, while a single high-frequency intramolecular mode ω_i, $\hbar\omega_i \gg kT$, is described quantum mechanically. Because ET occurs normally from the lowest vibrational level of the initial state, the rate k can be expressed as a sum over all channels connecting the initial state with the vibrational quantum number $n = 0$ to manifold vibrational levels of the final state [Eq. (10)]:

$$k = \sum_{n=0}^{\infty} k_{0 \to n}, \text{ where}$$

$$k_{0 \to n} = \frac{2\pi}{\hbar}V_{0 \to n}^2 \frac{1}{\sqrt{4\pi\lambda_s kT}} \exp\left[-\frac{(\Delta G + n\hbar\omega_i + \lambda_s)^2}{4\lambda_s kT}\right] \qquad (10)$$

$$\text{with } V_{0 \to n}^2 = V^2 \frac{S^n}{n!}\exp(-S)$$

An effective value of the Huang–Rhys factor S is estimated from the internal reorganization energy λ_i

$$S = \lambda_i / \hbar\omega_i$$

As seen, an additional parameter (as compared to the Marcus equation (9)) enters the semi-classical expression - the frequency ω_i of a vibrational mode that effectively describes the nuclear intramolecular relaxation following the ET. Typically, in organic systems, including fullerene, the main contribution to the internal reorganization energy is due to stretching of C=C bonds (the corresponding frequencies are in the range 1400–1800 cm^{-1}). Thus, the

effective frequency was set to 1600 cm^{-1}. It has been shown that varying the parameter ω_i within a reasonable range does not change significantly the computed ET rate.[19]

Reorganization energy

The reorganization energy is usually divided into two parts, $\lambda = \lambda_i + \lambda_s$, including the internal and solvent terms. The solvent reorganization energy corresponds to the energy required to move solvent molecules from the position they occupy in the GS to the location they have in the CT state, but without charge transfer having occurred. The λ_s for particular CT states were computed as a difference between equilibrium (Eq. (5)) and non-equilibrium (Eq. (7)) solvation energies. The internal reorganization energy λ_i corresponds to the energy of structural changes when the molecule goes from the initial-state geometry to the final-state geometry.

Interaction energies

The interaction energies were calculated directly from the electronic energy of the complex and the electronic energies of its subsystems. For **[10]CPP⊃C$_{60}$-XXX**, the interaction energy can be expressed as follows [Eq. (11)]:

$$E_{int} = E_{[10]CPP-C_{60}-XXX} - (E_{[10]CPP} + E_{C_{60}-XXX}) \qquad (11)$$

Energy decomposition analysis

The interaction energy in the gas phase is examined in the framework of the Kohn–Sham MO model using a quantitative energy decomposition analysis (EDA)[36] into electrostatic interactions, Pauli repulsive orbital interactions, and attractive orbital interactions, to which a term ΔE_{disp} is added to account for the dispersion correction [Eq. (12)]:

$$\Delta E_{int} = \Delta E_{elstat} + \Delta E_{Pauli} + \Delta E_{oi} + \Delta E_{disp} \qquad (12)$$

The term ΔV_{elstat} corresponds to the classical electrostatic interactions between the unperturbed charge distributions of the prepared (i.e., deformed) fragments and is usually attractive. The Pauli repulsion, ΔE_{Pauli}, comprises the destabilizing interactions between occupied orbitals and is responsible for any steric repulsion. The orbital interaction, ΔE_{oi}, accounts for electron-pair bonding, charge transfer (i.e., donor–acceptor interactions between occupied orbitals on one moiety and unoccupied orbitals on the other, including the HOMO-LUMO interactions) and polarization (empty-occupied orbital mixing on one fragment due to the presence of another fragment). The term ΔE_{disp} accounts for the dispersion corrections.[27]

Acknowledgements

Conflict of Interest

The authors declare no conflict of interest.

[1] a) Y. Xu, M. von Delius, *Angew. Chem. Int. Ed.* **2020**, *59*, 559–573; *Angew. Chem.* **2020**, *132*, 567–582; b) E. J. Leonhardt, R. Jasti, *Nat. Chem. Rev.* **2019**, *3*, 672–686; c) E. R. Darzi, R. Jasti, *Chem. Soc. Rev.* **2015**, *44*, 6401–6410.

[2] a) S. E. Lewis, *Chem. Soc. Rev.* **2015**, *44*, 2221–2304; b) D. Lu, Q. Huang, S. Wang, J. Wang, P. Huang, P. Du, *Front. Chem.* **2019**, *7*; c) Y. Segawa, A. Yagi, K. Itami, *Phys. Sci. Rev.* **2017**, *2*, 20160102.

[3] a) Y. Segawa, H. Omachi, K. Itami, *Org. Lett.* **2010**, *12*, 2262–2265; b) H. Omachi, Y. Matsuura, Y. Segawa, K. Itami, *Angew. Chem. Int. Ed.* **2010**, *49*, 10202–10205; *Angew. Chem.* **2010**, *122*, 10400–10403.

[4] a) Y. Xu, B. Wang, R. Kaur, M. B. Minameyer, M. Bothe, T. Drewello, D. M. Guldi, M. von Delius, *Angew. Chem. Int. Ed.* **2018**, *57*, 11549–11553; *Angew. Chem.* **2018**, *130*, 11723–11727; b) Y. Xu, R. Kaur, B. Wang, M. B. Minameyer, S. Gsänger, B. Meyer, T. Drewello, D. M. Guldi, M. von Delius, *J. Am. Chem. Soc.* **2018**, *140*, 13413–13420; c) D. Wu, W. Cheng, X. Ban, J. Xia, *Asian J. Org. Chem.* **2018**, *7*, 2161–2181; d) S. Toyota, E. Tsurumaki, *Chem. Eur. J.* **2019**, *25*, 6878–6890.

[5] T. Iwamoto, Y. Watanabe, T. Sadahiro, T. Haino, S. Yamago, *Angew. Chem. Int. Ed.* **2011**, *50*, 8342–8344; *Angew. Chem.* **2011**, *123*, 8492–8494.

[6] a) Y. Nakanishi, H. Omachi, S. Matsuura, Y. Miyata, R. Kitaura, Y. Segawa, K. Itami, H. Shinohara, *Angew. Chem. Int. Ed.* **2014**, *53*, 3102–3106; *Angew. Chem.* **2014**, *126*, 3166–3170; b) Q. Huang, G. Zhuang, H. Jia, M. Qian, S. Cui, S. Yang, P. Du, *Angew. Chem. Int. Ed.* **2019**, *58*, 6244–6249; *Angew. Chem.* **2019**, *131*, 6310–6315; c) T. Iwamoto, Y. Watanabe, H. Takaya, T. Haino, N. Yasuda, S. Yamago, *Chem. Eur. J.* **2013**, *19*, 14061–14068; d) J. Rio, S. Beeck, G. Rotas, S. Ahles, D. Jacquemin, N. Tagmatarchis, C. Ewels, H. A. Wegner, *Angew. Chem. Int. Ed.* **2018**, *57*, 6930–6934; *Angew. Chem.* **2018**, *130*, 7046–7050; e) S. Cui, G. Zhuang, D. Lu, Q. Huang, H. Jia, Y. Wang, S. Yang, P. Du, *Angew. Chem. Int. Ed.* **2018**, *57*, 9330–9335; *Angew. Chem.* **2018**, *130*, 9474–9479; f) E. Ubasart, O. Borodin, C. Fuertes-Espinosa, Y. Xu, C. García-Simón, L. Gómez, J. Juanhuix, F. Gándara, I. Imaz, D. Maspoch, M. Von Delius, X. Ribas, *Nature Chem.* **2021**, *13*, 420–427.

[7] a) H. Isobe, S. Hitosugi, T. Yamasaki, R. Iizuka, *Chem. Sci.* **2013**, *4*, 1293–1297; b) S. Hitosugi, K. Ohkubo, R. Iizuka, Y. Kawashima, K. Nakamura, S. Sato, H. Kono, S. Fukuzumi, H. Isobe, *Org. Lett.* **2014**, *16*, 3352–3355.

[8] H. Isobe, K. Nakamura, S. Hitosugi, S. Sato, H. Tokoyama, H. Yamakado, K. Ohno, H. Kono, *Chem. Sci.* **2015**, *6*, 2746–2753.

[9] H. Ueno, T. Nishihara, Y. Segawa, K. Itami, *Angew. Chem. Int. Ed.* **2015**, *54*, 3707–3711; *Angew. Chem.* **2015**, *127*, 3778–3782.

[10] A. J. Stasyuk, O. A. Stasyuk, M. Solà, A. A. Voityuk, *Chem. Commun.* **2019**, *55*, 11195–11198.

[11] K. Morokuma, *J. Chem. Phys.* **1971**, *55*, 1236–1244.

[12] a) G. te Velde, F. M. Bickelhaupt, E. J. Baerends, C. Fonseca Guerra, S. J. A. van Gisbergen, J. G. Snijders, T. Ziegler, *J. Comput. Chem.* **2001**, *22*, 931–967; b) ADF 2019, SCM, Theoretical Chemistry, Vrije Universiteit, Amsterdam, The Netherlands, http://www.scm.com.

[13] A. J. Stasyuk, O. A. Stasyuk, M. Solà, A. A. Voityuk, *J. Phys. Chem. C* **2019**, *123*, 16525–16532.

[14] A. J. Stasyuk, O. A. Stasyuk, M. Solà, A. A. Voityuk, *J. Phys. Chem. B* **2020**, *124*, 9095–9102.

[15] a) J. Tomasi, B. Mennucci, R. Cammi, *Chem. Rev.* **2005**, *105*, 2999–3094; b) A. J. Stasyuk, O. A. Stasyuk, M. Solà, A. A. Voityuk, *Phys. Chem. Chem. Phys.* **2019**, *21*, 25098–25107; c) A. J. Stasyuk, O. A. Stasyuk, M. Solà, A. A. Voityuk, *Chem. Eur. J.* **2020**, *26*, 10896–10902.

[16] J. A. Luque-Urrutia, A. Poater, M. Solà, *Chem. Eur. J.* **2020**, *26*, 804–808.

[17] B. Mennucci, *WIREs Comput. Mol. Sci.* **2012**, *2*, 386–404.

[18] J. Ulstrup, J. Jortner, *J. Chem. Phys.* **1975**, *63*, 4358–4368.

[19] a) T. Liu, A. Troisi, *J. Phys. Chem. C* **2011**, *115*, 2406–2415; b) A. J. Stasyuk, O. A. Stasyuk, M. Solà, A. A. Voityuk, *Chem. Commun.* **2020**, *56*, 12624–12627.

[20] a) A. D. Becke, *Phys. Rev. A* **1988**, *38*, 3098–3100; b) C. Lee, W. Yang, R. G. Parr, *Phys. Rev. B* **1988**, *37*, 785–789.

[21] a) F. Weigend, R. Ahlrichs, *Phys. Chem. Chem. Phys.* **2005**, *7*, 3297–3305; b) F. Weigend, *Phys. Chem. Chem. Phys.* **2006**, *8*, 1057–1065.

[22] a) K. Eichkorn, O. Treutler, H. Öhm, M. Häser, R. Ahlrichs, *Chem. Phys. Lett.* **1995**, *240*, 283–290; b) K. Eichkorn, F. Weigend, O. Treutler, R. Ahlrichs, *Theor. Chem. Acc.* **1997**, *97*, 119–124.

[23] a) F. Neese, *WIREs Comput. Mol. Sci.* **2012**, *2*, 73–78; b) F. Neese, *WIREs Comput. Mol. Sci.* **2018**, *8*, e1327.

[24] S. Hirata, M. Head-Gordon, *Chem. Phys. Lett.* **1999**, *314*, 291–299.

[25] T. Yanai, D. P. Tew, N. C. Handy, *Chem. Phys. Lett.* **2004**, *393*, 51–57.

[26] Gaussian 16, Revision A.03, M. J. Frisch, G. W. Trucks, H. B. Schlegel, G. E. Scuseria, M. A. Robb, J. R. Cheeseman, G. Scalmani, V. Barone, G. A. Petersson, H. Nakatsuji, X. Li, M. Caricato, A. V. Marenich, J. Bloino, B. G. Janesko, R. Gomperts, B. Mennucci, H. P. Hratchian, J. V. Ortiz, A. F. Izmaylov, J. L. Sonnenberg, D. Williams-Young, F. Ding, F. Lipparini, F. Egidi, J. Goings, B. Peng, A. Petrone, T. Henderson, D. Ranasinghe, V. G. Zakrzewski, J. Gao, N. Rega, G. Zheng, W. Liang, M. Hada, M. Ehara, K. Toyota, R. Fukuda, J. Hasegawa, M. Ishida, T. Nakajima, Y. Honda, O. Kitao, H. Nakai, T. Vreven, K. Throssell, J. A. Montgomery, Jr., J. E. Peralta, F. Ogliaro, M. J. Bearpark, J. J. Heyd, E. N. Brothers, K. N. Kudin, V. N. Staroverov, T. A. Keith, R. Kobayashi, J. Normand, K. Raghavachari, A. P. Rendell, J. C. Burant, S. S. Iyengar, J. Tomasi, M. Cossi, J. M. Millam, M. Klene, C. Adamo, R. Cammi, J. W. Ochterski, R. L. Martin, K. Morokuma, O. Farkas, J. B. Foresman, D. J. Fox, Gaussian, Inc., Wallingford CT, **2016**.

[27] a) S. Grimme, J. Antony, S. Ehrlich, H. Krieg, *J. Chem. Phys.* **2010**, *132*, 154104; b) S. Grimme, S. Ehrlich, L. Goerigk, *J. Comput. Chem.* **2011**, *32*, 1456–1465.

[28] G. A. Zhurko, Chemcraft 1.80 (build 523b) - graphical program for visualization of quantum chemistry computations. (https://chemcraft-prog.com).

[29] a) F. Plasser, H. Lischka, *J. Chem. Theory Comput.* **2012**, *8*, 2777–2789; b) F. Plasser, S. A. Bäppler, M. Wormit, A. Dreuw, *J. Chem. Phys.* **2014**, *141*, 024107; c) A. V. Luzanov, O. A. Zhikol, *Int. J. Quantum Chem.* **2010**, *110*, 902–924.

[30] A. Klamt, G. Schüürmann, *J. Chem. Soc. Perkin Trans. 2* **1993**, 799–805.

[31] J. L. Pascual-ahuir, E. Silla, I. Tuñon, *J. Comput. Chem.* **1994**, *15*, 1127–1138.

[32] A. Klamt, *J. Phys. Chem.* **1996**, *100*, 3349–3353.

[33] R. A. Marcus, N. Sutin, *Biochim. Biophys. Acta Bioenerg.* **1985**, *811*, 265–322.

[34] a) A. A. Voityuk, N. Rösch, *J. Chem. Phys.* **2002**, *117*, 5607–5616; b) A. A. Voityuk, *Phys. Chem. Chem. Phys.* **2012**, *14*, 13789–13793.

[35] J. Jortner, *J. Chem. Phys.* **1976**, *64*, 4860–4867.

[36] a) T. Ziegler, A. Rauk, *Theor. Chim. Acta* **1977**, *46*, 1–10; b) T. Ziegler, A. Rauk, *Inorg. Chem.* **1979**, *18*, 1558–1565.